


RESEARCH ARTICLE

Recovery of left ventricular function following in vivo reexpression of cardiac myosin binding protein C

Jasmine Giles¹, Jitandrakumar R. Patel^{1,2}, Adam Miller¹, Elizabeth Iverson¹, Daniel Fitzsimons^{1,2}, and Richard L. Moss^{1,2} 

The loss of cardiac myosin binding protein C (cMyBP-C) results in left ventricular dilation, cardiac hypertrophy, and impaired ventricular function in both constitutive and conditional cMyBP-C knockout (*MYBPC3* null) mice. It remains unclear whether the structural and functional phenotypes expressed in the *MYBPC3* null mouse are reversible, which is an important question, since reduced expression of cMyBP-C is an important cause of hypertrophic cardiomyopathy in humans. To investigate this question, we generated a cardiac-specific transgenic mouse model using a Tet-Off inducible system to permit the controlled expression of WT cMyBP-C on the *MYBPC3* null background. Functional Tet-Off mice expressing WT cMyBP-C (FT-WT) were generated by crossing tetracycline transactivator mice with responder mice carrying the WT cMyBP-C transgene. Prior to dietary doxycycline administration, cMyBP-C was expressed at normal levels in FT-WT myocardium, which exhibited similar levels of steady-state force and in vivo left ventricular function as WT mice. Introduction of dietary doxycycline for four weeks resulted in a partial knockdown of cMyBP-C expression and commensurate impairment of systolic and diastolic function to levels approaching those observed in *MYBPC3* null mice. Subsequent withdrawal of doxycycline from the diet resulted in the reexpression of cMyBP-C to levels comparable to those observed in WT mice, along with near-complete recovery of in vivo ventricular function. These results show that the cardiac phenotypes associated with *MYBPC3* null mice are reversible. Our work also validates the use of the Tet-Off inducible system as a means to study the mechanisms underlying hypertrophic cardiomyopathy.

Introduction

Myosin binding protein C (MyBP-C) is a key thick-filament-associated regulatory protein in vertebrate skeletal and cardiac muscles (Offer et al., 1973; Bennett et al., 1999; Winegrad, 1999). The cardiac isoform (cardiac myosin binding protein C [cMyBP-C]) contains eight immunoglobulin-like and three fibronectin-like structural domains, designated C0–C10. A unique cardiac-specific motif sequence, located between domains C1 and C2, contains three protein kinase A phosphorylatable serine residues, one of which is also phosphorylated by CaM kinase II. While the C-terminal domains anchor cMyBP-C to the thick filament (Flashman et al., 2004), the N-terminal domains have been shown to interact with myosin subfragment 2 (Gruen and Gautel, 1999; Ababou et al., 2007, 2008; Ratti et al., 2011; Bhuiyan et al., 2016) and the thin filament (Weith et al., 2012b; Bezold et al., 2013; van Dijk et al., 2014) in a phosphorylation-dependent manner (Weith et al., 2012a; Previs et al., 2016; Kensler et al., 2017). Collectively, the cMyBP-C N-terminal interactions modulate the activation state of the cardiac thin filament (Previs et al., 2012; Kampourakis et

al., 2014; Mun et al., 2014), thereby allowing cMyBP-C to play an essential role in augmenting myocardial contractility, particularly in response to β -adrenergic stimulation (Sadayappan et al., 2011; Tong et al., 2015; Gresham et al., 2017; Mamidi et al., 2017).

Hypertrophic cardiomyopathy (HCM) is an autosomal-dominant disease of cardiac muscle characterized by in vivo left ventricular (LV) dysfunction and aberrant myocardial structure. To date, the most common site of HCM-related mutations is *MYBPC3* (Harris et al., 2011; Carrier et al., 2015), the gene that encodes for cMyBP-C. The majority of *MYBPC3* mutations encode C-terminal truncations of cMyBP-C (Carrier et al., 2015) that lack the binding domains responsible for anchoring cMyBP-C to the thick filament. Mutations in cMyBP-C are characterized by highly variable manifestations of HCM disease phenotypes and risk for arrhythmias, ranging in severity from a life-long asymptomatic state to sudden cardiac arrest in childhood (Van Driest et al., 2004).

How these HCM-related cMyBP-C mutations elicit cardiac disease remains relatively unknown. To help address this issue,

¹Department of Cell and Regenerative Biology, University of Wisconsin School of Medicine and Public Health, University of Wisconsin–Madison, Madison, WI; ²University of Wisconsin Cardiovascular Research Center, University of Wisconsin School of Medicine and Public Health, University of Wisconsin–Madison, Madison, WI.

Correspondence to Richard L. Moss: rlmoss@wisc.edu.

This work is part of a special collection on myofilament function.

© 2018 Giles et al. This article is distributed under the terms of an Attribution–Noncommercial–Share Alike–No Mirror Sites license for the first six months after the publication date (see <http://www.rupress.org/terms/>). After six months it is available under a Creative Commons License (Attribution–Noncommercial–Share Alike 4.0 International license, as described at <https://creativecommons.org/licenses/by-nc-sa/4.0/>).

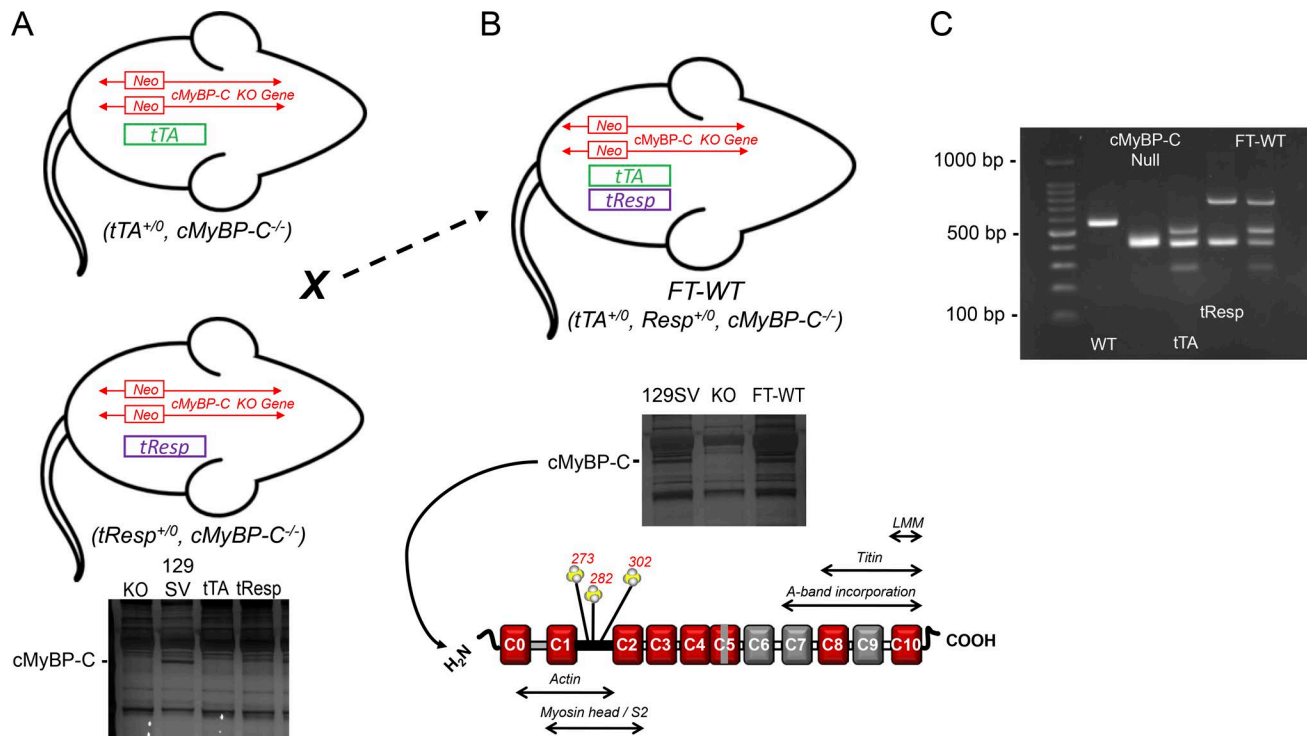


Figure 1. Generation of Tet-Off inducible mice expressing WT cMyBP-C. (A) Mice, hemizygous for the *tTA* transgene (Sanbe et al., 2003) and homozygous for endogenous *cMyBP-C* ($tTA^{+/-}$, $cMyBP-C^{-/-}$), were backcrossed for five successive generations with *cMyBP-C* null ($cMyBP-C^{-/-}$) mice to generate the *tTA* mouse line ($tTA^{+/-}$, $cMyBP-C^{-/-}$) used in this study. The same strategy was used to generate the *tResp* transgenic mouse line on the *cMyBP-C* null background ($tResp^{+/-}$, $cMyBP-C^{-/-}$). Neither the *tTA* mice nor the *tResp* mice expressed cMyBP-C (bottom). (B) The *tTA* and *tResp* lines were subsequently crossed to generate the double-transgenic mouse (FT-WT). Approximately 25% of the resulting progeny were hemizygous for both transgenes ($tTA^{+/-}$, $tResp^{+/-}$, $cMyBP-C^{-/-}$) and expressed WT cMyBP-C (bottom). (C) PCR genotyping strategy used to generate FT-WT mice. Shown are PCR products amplified from genomic DNA isolated from WT ($cMyBP-C^{+/+}$), *cMyBP-C* null ($cMyBP-C^{-/-}$), *tTA* ($tTA^{+/-}$, $cMyBP-C^{-/-}$), *tResp* ($tResp^{+/-}$, $cMyBP-C^{-/-}$), and FT-WT ($tTA^{+/-}$, $tResp^{+/-}$, $cMyBP-C^{-/-}$) mice.

several unique mouse models were generated to determine the effect of either eliminating cMyBP-C expression (Harris et al., 2002; Carrier et al., 2004) or expressing low levels of truncated cMyBP-C (McConnell et al., 1999) in order to gain insight into the disease processes associated with HCM. Collectively, these models have demonstrated the deleterious effects of ablation (cMyBP-C null) or reduced expression of cMyBP-C in the murine heart, as evidenced by decreased in vivo LV systolic contractility, prolonged LV relaxation, marked cardiac hypertrophy, and LV dilation. However, it is unclear whether the direct loss of cMyBP-C, which was initiated in utero, or the compensatory development of cardiac hypertrophy during neonatal development (de Lange et al., 2013) is the primary mechanism underlying the LV functional deficits. The tamoxifen-inducible cMyBP-C conditional knockout mouse model (Chen et al., 2012) was subsequently developed and demonstrated that the direct loss of cMyBP-C and associated LV dysfunction in adult mice preceded the development of cardiac hypertrophy and cytoarchitectural remodeling.

Both the constitutive and conditional cMyBP-C null mouse models are limited in terms of investigating the phenotypic effects associated with the loss of cMyBP-C.

Thus, to further our understanding of the phenotypic changes associated with the cMyBP-C null mouse and determine the degree to which these phenotypic changes are reversible, we used a Tet-Off inducible system (Sanbe et al., 2003) to permit controlled transgenic expression of WT cMyBP-C on the cMyBP-C

null background (FT-WT). Introduction of dietary doxycycline at 3–6 mo of age resulted in the partial knockdown of cMyBP-C expression and concomitant derangements of LV systolic and diastolic function. The subsequent withdrawal of doxycycline from the diet resulted in the reexpression of cMyBP-C and near-complete recovery of LV function, validating the feasibility of using the Tet-Off inducible mouse model to study the disease mechanisms underlying HCM-related cMyBP-C mutations.

Materials and methods

Experimental animals

We generated a cardiac-specific transgenic mouse model using a Tet-Off inducible system (Sanbe et al., 2003; Razzaque et al., 2013) to permit the expression of WT cMyBP-C on the *MYBPC3* null background. In brief, the controlled expression of cMyBP-C requires the presence of (1) a tetracycline-controlled transactivator (*tTA*) transgene, in which an α -MyHC promoter is coupled to the transcription activator virion protein 16 sequence; and (2) a responder (*tResp*) transgene, in which a cytomegalovirus minimal promoter is coupled to the Tet operon ligated to the WT cMyBP-C complementary DNA. Mice hemizygous (Gulick and Robbins, 2005) for the *tTA* and *tResp* transgenes were initially crossed with *cMyBP-C* null ($cMyBP-C^{-/-}$) mice to eliminate the endogenous expression of cMyBP-C. The subsequent breeding of mice homozygous for *cMyBP-C* null and hemizygous for the

tTA transgene ($tTA^{+/0}$, $cMyBP-C^{-/-}$) with mice homozygous for cMyBP-C null and hemizygous for the cMyBP-C tResp transgene ($tResp^{+/0}$, $cMyBP-C^{-/-}$) generated the double-transgenic mouse (FT-WT: $tTA^{+/0}$, $tResp^{+/0}$, $cMyBP-C^{-/-}$), which stably expressed WT cMyBP-C (Fig. 1). This breeding scheme generated progeny close to the predicted frequency of 25%, i.e., $cMyBP-C^{-/-}$ (23.0%); $cMyBP-C^{-/-}$, $tTA^{+/0}$ (22.9%); $cMyBP-C^{-/-}$, $tResp^{+/0}$ (29.5%); and $cMyBP-C^{-/-}$, $tTA^{+/0}$, $tResp^{+/0}$ (24.6%). To elicit the transient knock-down of cMyBP-C expression, FT-WT mice of either sex were fed normal rodent chow supplemented with 1,250 mg/kg doxycycline for a total of 4 wk. Reexpression of cMyBP-C in the FT-WT mice was induced by returning these animals to a diet of normal rodent chow. All procedures for animal care, handling, and use were reviewed and approved by the Animal Care and Use Committee of the University of Wisconsin School of Medicine and Public Health.

Steady-state mechanical measurements

Solutions

Solution compositions were calculated using the computer program of [Fabiato \(1988\)](#) and stability constants ([Godt and Lindley, 1982](#)) corrected to pH 7.0 and 22°C for all solutions. The composition of relaxing solution was (in mM) 100 KCl, 20 imidazole, 4 MgATP, 2 EGTA, and 1 free Mg^{2+} . The composition of preactivating solution was (in mM) 100 BES, 15 creatine phosphate, 5 dithiothreitol, 4 MgATP, 1 free Mg^{2+} , and 0.07 EGTA. Activating solution contained (in mM) 100 BES, 15 creatine phosphate, 7 EGTA, 5 dithiothreitol, 4 MgATP, 1 free Mg^{2+} , with $[Ca^{2+}]_{free}$ ranging from 1 nM (i.e., pCa 9.0) to 32 μ M (i.e., pCa 4.5). A range of submaximal pCa solutions containing different $[Ca^{2+}]_{free}$ were prepared by mixing pCa 9.0 and pCa 4.5 solutions. The ionic strength of preactivating and activating solutions was adjusted to 180 mM using potassium propionate.

Isolation of right ventricular trabeculae

Hearts were rapidly excised from mice of either sex (3–9 mo old) previously injected with 5,000 U heparin/kg body weight and anesthetized with isoflurane. The left and right ventricles were separated at the septum, pinned down to the base of the dissecting dish, and perfused with a Ca^{2+} -Ringer's solution (in mM: 120 NaCl, 19 $NaHCO_3$, 10 glucose, 5 KCl, 1.2 Na_2HPO_4 , 1.2 $MgSO_4$, 1 $CaCl_2$, and 30 2,3-butanedione monoxime, pH 7.4 and 22°C) preequilibrated with 95% O_2 /5% CO_2 . After 30 min, the ventricles were rapidly frozen in liquid nitrogen and stored at $-80^\circ C$ until used. Skinned right ventricular trabeculae were prepared for use in steady-state mechanical measurements, as described previously ([Patel et al., 2012](#)). In brief, the frozen ventricles were thawed in ice-cold relaxing solution and subsequently cut open. The exposed trabeculae were dissected free, tied to sticks to hold muscle length fixed, and transferred to fresh, ice-cold relaxing solution containing 1% Triton X-100 and 0.25 mg/ml saponin for 60 min. The trabeculae were subsequently transferred to fresh, ice-cold relaxing solution and used for mechanical measurements within 2–3 h.

Experimental apparatus

Before each experiment, the ends of an individual trabecula (dimensions: $750\text{--}1,000 \times 150\text{--}250 \mu m$) were trimmed and mounted

between a force transducer (model 403; Aurora Scientific) and a DC torque motor (model 312B; Aurora Scientific). The apparatus was placed on the stage of an inverted microscope (Olympus) fitted with a $\times 40$ objective and a CCTV camera (model WV-BL600; Panasonic). The light from a halogen lamp was used to illuminate the skinned trabeculae. Bitmap images of the skinned trabeculae were acquired using an AGP $4 \times / 2 \times$ graphics card and associated software (ATI Technologies) and were used to measure mean sarcomere length and fiber dimensions during activation and relaxation. All experiments were performed at 22°C and at a sarcomere length of $\sim 2.20 \mu m$ in pCa 9.0 solution. Changes in force and motor position were sampled (16-bit resolution, DAP5216a; Microstar Laboratories) at 2.0 kHz using SLControl software (<http://www.slcontrol.com>). All data were saved to computer files for subsequent analysis.

Rate of force redevelopment

The rate constant of force redevelopment (k_{tr}) in skinned trabeculae was assessed as previously described ([Fitzsimons et al., 2001](#)). Measurement of k_{tr} involves a mechanical slack-restretch maneuver to dissociate bound myosin cross-bridges from actin in a steadily Ca^{2+} -activated preparation. Each skinned trabecula was transferred from pCa 9.0 to activating solutions of varying pCa (i.e., pCa 6.2–4.5) and allowed to generate steady-state force. The trabecula was then rapidly (< 2 ms) slackened by 20% of its original length, resulting in an abrupt reduction of force to near zero, followed by a brief period (~ 14 ms) of unloaded shortening, after which the preparation was restretched rapidly (< 2 ms) to its initial length. Force redevelopment following the slack-restretch maneuver reflects the rate of cross-bridge cycling between weakly bound and strongly bound force-generating states. A k_{tr} -pCa relationship was obtained by first maximally activating the skinned trabeculae in a solution of pCa 4.5 and then in a series of submaximally activating solutions between pCa 6.2–5.3. To assess any decline in maximal k_{tr} , the trabecula was activated in a solution of pCa 4.5 at the end of each experiment. The apparent rate constants of force redevelopment were estimated by linear transformation of the half-time of force redevelopment, i.e., $k_{tr} = 0.693 / t_{1/2}$ ([Fitzsimons et al., 2001](#)).

Force-pCa relationship

During measurements of k_{tr} , each trabecula was exposed to solutions of varying pCa and allowed to develop steady-state force. The difference between steady-state force and the force baseline after the slack step was measured as the total force at that pCa. Active force was obtained by subtracting Ca^{2+} -independent force, measured in solution of pCa 9.0, from the total force. Force-pCa relationships were determined by expressing submaximal force (P) at each pCa as a fraction of maximal force (P_0) determined in pCa 4.5, i.e., P/P_0 . The force-pCa data were fit using the equation $P/P_0 = [Ca^{2+}]^n / (k^n + [Ca^{2+}]^n)$, where n is the Hill coefficient and k is the $[Ca^{2+}]$ required for half-maximal activation (pCa₅₀). Hill plot transformations of the force-pCa data were generated using the following equation: $\log[P_{rel}/(1 - P_{rel})] = n(\log[Ca^{2+}] + k)$, where P_{rel} is force expressed as a fraction of P_0 , n is the Hill coefficient, and k is the $[Ca^{2+}]$ required for half-maximal activation (pCa₅₀).

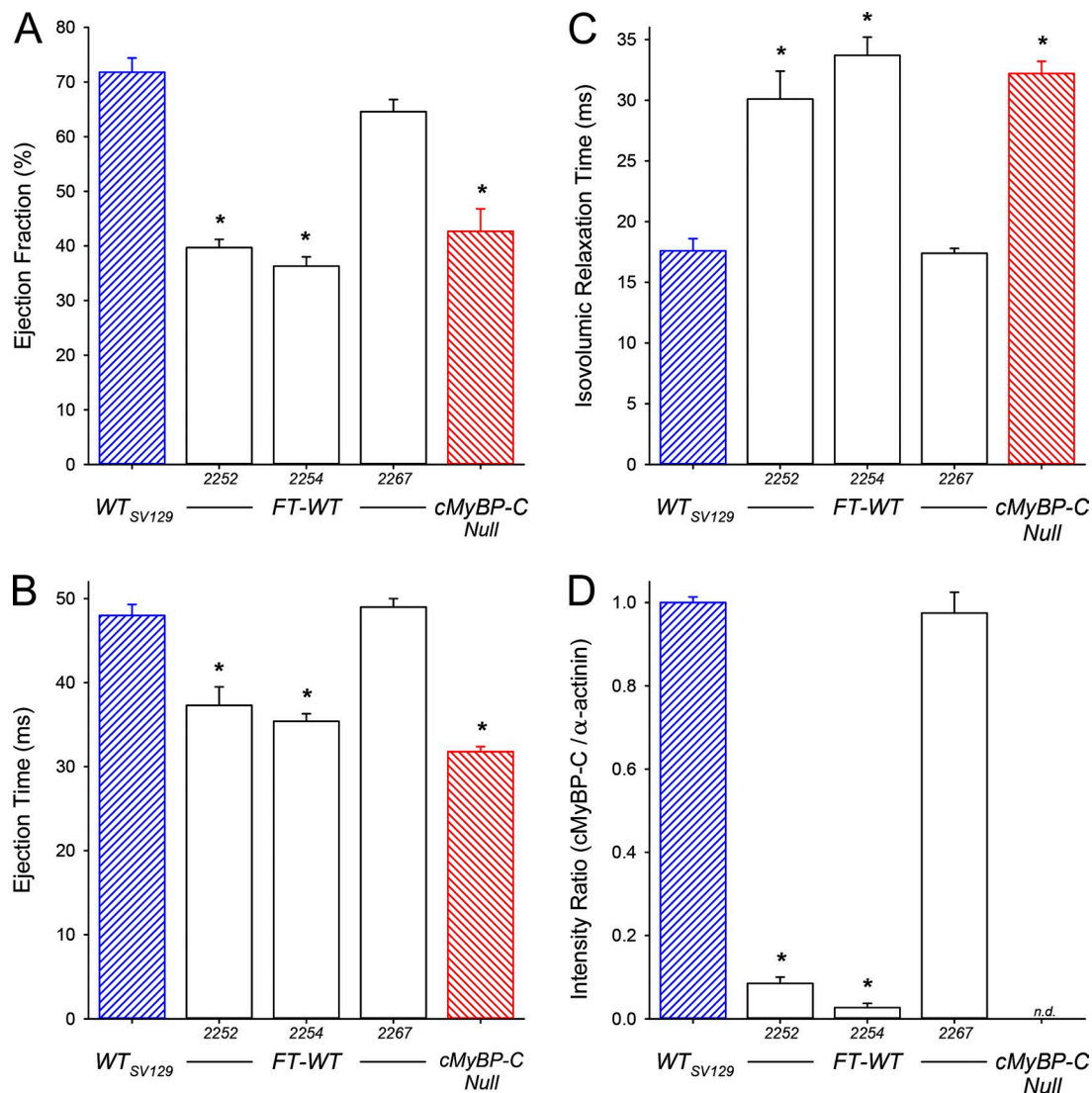


Figure 2. **Selection of the inducible FT-WT mouse line.** (A–D) All values represent means, and error bars represent \pm SEM, with $n = 3$ animals per group. Echocardiographic analysis of LV EF (A), ET (B), IVRT (C), and relative expression of cMyBP-C (D) in WT, cMyBP-C null, and FT-WT (sublines 2252, 2254, and 2267) mice. *, $P < 0.05$ significant difference of FT-WT and cMyBP-C null mice versus WT mice.

Echocardiography

Serial echocardiograms were performed on FT-WT mice before ($t = 0$), during ($t = 2$ and 4 wk), and after ($t = 1, 4, 8$, and 16 wk) dietary supplementation with doxycycline. Age-matched WT and cMyBP-C null mice were also subjected to echocardiographic analysis and served as additional controls. Transthoracic echocardiographs were performed using a VisualSonics Vevo7770 high-resolution imaging system (Chen et al., 2012). The mice were lightly anesthetized with 1% isoflurane (inhaled) and maintained on a heated platform at 37°C . Two-dimensional M-mode images of the left ventricle were collected to produce LV internal dimension in diastole (LVID_d) and systole (LVID_s), LV posterior wall thickness in diastole (LVPW_d), systole (LVPW_s), and isovolumic relaxation time (IVRT). Endocardial fractional shortening was calculated as $[(\text{LVID}_d - \text{LVID}_s)/\text{LVID}_d \times 100]$, and ejection fraction (EF) was calculated as $[(\text{LV Vol}_d - \text{LV Vol}_s)/\text{LV Vol}_d \times 100]$. Systolic ejection time (ET) and heart rate were measured from pulse-wave Doppler tracings of the LV outflow tract recorded in

the suprasternal view. All echocardiographic parameters were measured over at least three consecutive cycles, with a minimum of eight mice per group.

Immunohistochemistry

Surgically excised WT ($n = 3$), cMyBP-C^{-/-} null ($n = 3$), and noninduced FT-WT ($n = 3$) hearts were cannulated and perfused with Ca^{2+} -free Ringer's solution in a Langendorff perfusion setup for 30 min and then subsequently fixed with 10% neutral-buffered formalin for 24 h. Cross-sectional views along the coronal plane were obtained from paraffin-embedded samples sectioned at $5 \mu\text{m}$. The resulting sections were stained with hematoxylin and eosin to detect any nuclear and cytoplasmic abnormalities and Masson's trichrome to visualize any evidence of interstitial fibrosis. The extent of fibrosis in cardiac tissue was analyzed using ImageJ 1.52a software (National Institutes of Health). The results were expressed as a percent ratio of the fibrotic area relative to the entire cross section. Additional sections were deparaffinized,

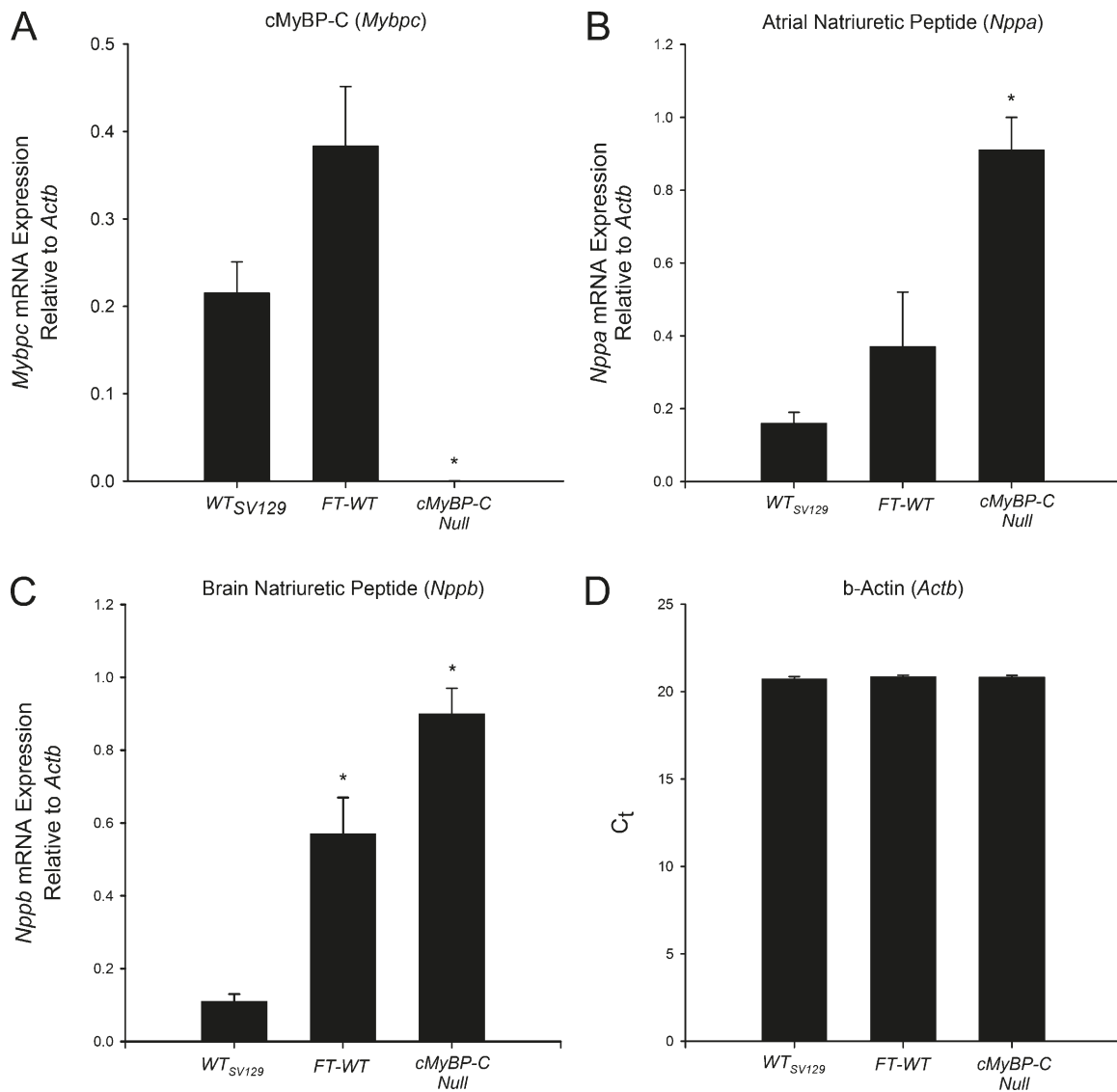


Figure 3. **Gene expression in FT-WT hearts.** (A–D) The relative expression of *MYBPC3* (A), atrial natriuretic peptide (B), and brain natriuretic peptide mRNA (C) was normalized to β -actin (D) in FT-WT, WT and cMyBP-C null hearts. All values represent means, and error bars represent SEM, with values obtained in triplicate from three hearts per group. *, $P < 0.05$ significant difference of FT-WT and cMyBP-C null mice versus WT mice.

rehydrated, and incubated (1:400 dilution) with a polyclonal antibody raised against cMyBP-C (Harris et al., 2002) in a humidified chamber at 4°C for 16 h. Immunofluorescent detection of cMyBP-C was performed by using a goat anti-rabbit secondary antibody conjugated to Alexa Fluor 488 (1:10,000 dilution; ThermoFisher) and counterstained with DAPI. All sections were imaged on a Leica SP8 3X STED super-resolution microscope provided by the Optical Imaging Core facility at the University of Wisconsin School of Medicine and Public Health.

PAGE

Preparation of myofibrillar proteins

To determine the relative expression levels of cMyBP-C, myofibrillar proteins were extracted from WT, cMyBP-C null, and FT-WT frozen ventricles (Chen et al., 2010). In brief, the frozen ventricles were pulverized under liquid nitrogen and homogenized in fresh, ice-cold relaxing solution and centrifuged. The

resulting pellet was resuspended in fresh, ice-cold relaxing solution containing 1% Triton X-100 and 0.25 mg/ml saponin for 30 min at room temperature and then centrifuged. The myofibrillar pellet was washed and centrifuged three times in fresh, ice-cold relaxing solution. The final myofibrillar pellet was solubilized in SDS sample buffer containing (in mM) 62.5 mM Tris-HCl, 15% glycerol, 5 mM dithiothreitol, and 2% SDS, pH 6.8. A BCA Protein Assay (Pierce) was used to determine the myofibrillar protein concentration of each sample.

SDS-PAGE

Myofibrillar proteins were loaded onto 10% Tris-HCl criterion gels (Bio-Rad), electrophoresed at 150 V (constant voltage) for 90 min at room temperature, and silver stained (Patel et al., 2017). Densitometric analysis was performed using Image Lab software (Bio-Rad), with the intensity ratio of the integrated optical density (IOD) band of the cMyBP-C band to the IOD of the cor-

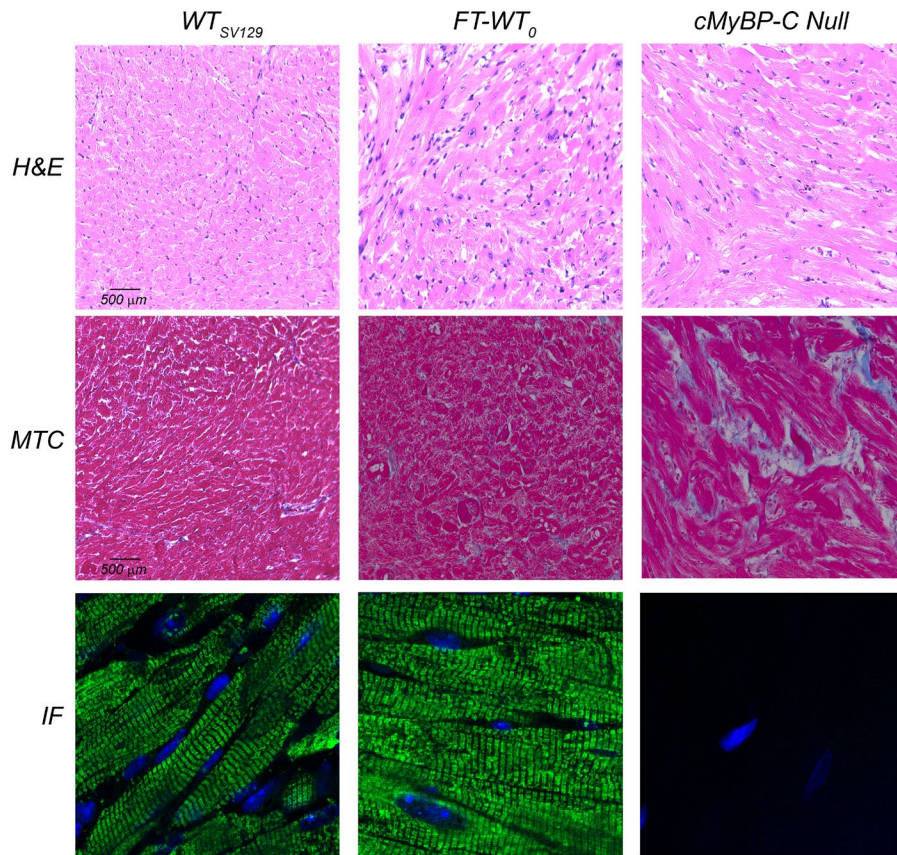


Figure 4. **FT-WT mice exhibit normal cardiac histology and correct sarcomeric incorporation of cMyBP-C.** Representative high-magnification ($\times 400$) photomicrographs of hematoxylin and eosin (H&E)-stained sections (top row) and Masson's trichrome (MTC)-stained sections (middle row), demonstrating the absence of overt fibrosis in the FT-WT myocardium. Representative confocal images (IF; bottom row) of both WT and FT-WT cardiac sections demonstrate the classic A-band doublet staining of cMyBP-C.

responding α -actinin band calculated to correct for loading and to permit comparison between samples. All cMyBP-C/ α -actinin intensity ratios were normalized to WT values.

Western blot analysis

Myofibrillar proteins were resolved on 10% Tris-HCl Criterion gels (Bio-Rad) and transferred onto a nitrocellulose membranes overnight at 4°C . The membranes were blocked with 5% nonfat

milk for 60 min on a shaker and then incubated with a rabbit polyclonal antibody raised against cMyBP-C (1:1,000 dilution) and a mouse monoclonal antibody raised against β -actin (1:5,000 dilution; Sigma Aldrich) overnight at 4°C , followed by three washes in Tris-buffered saline Tween buffer. The membranes were then incubated with goat anti-rabbit IgG (1:10,000 dilution) and goat anti-mouse IgG (1:5,000 dilution) each conjugated to Alexa Fluor 647 (ThermoFisher). Western blot images were taken with the

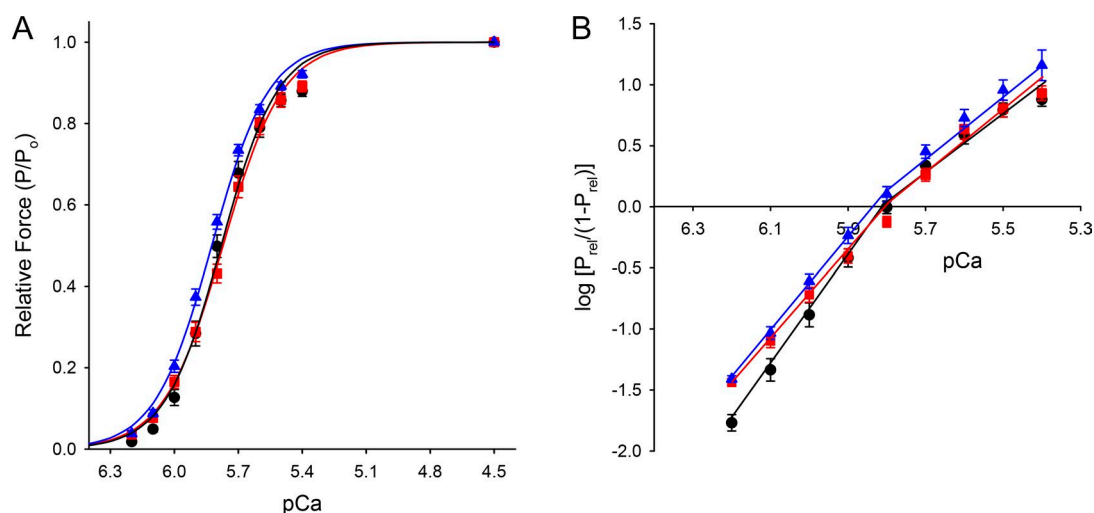


Figure 5. **Steady-state force development in FT-WT skinned myocardium.** (A and B) Ca^{2+} -activated force- $p\text{Ca}$ relationship (A) and Hill plot transformations of the force- $p\text{Ca}$ data (B) were measured in skinned trabeculae from WT (triangle), FT-WT (circle), and cMyBP-C null (square) mice. All values represent means, and error bars represent $\pm \text{SEM}$, with summary data listed in Table 1.

Table 1. Summary of steady-state mechanical measurements

Measurement	WT _{SV129} (9)	FT-WT ₀ (8)	cMyBP-C null (8)
P_{Tot} (mN/mm ²)	39.8 ± 3.6	30.1 ± 5.2	21.7 ± 3.1
P_o (mN/mm ²)	38.1 ± 3.6	27.9 ± 5.2	19.8 ± 3.0
P_{rest} (mN/mm ²)	1.7 ± 0.2	2.2 ± 0.3	1.9 ± 0.2
% P_{rest}	4.3 ± 0.1	8.6 ± 1.6	9.7 ± 1.9
n_H	3.4 ± 0.1	3.4 ± 0.1	3.2 ± 0.2
pCa_{50}	5.82 ± 0.02	5.78 ± 0.02	5.77 ± 0.02
ktr (s ⁻¹)	25.9 ± 2.0	29.3 ± 1.2	38.2 ± 1.7 ^a

All values are expressed as means ± SEM, with the number of trabecular preparations listed in parentheses. ktr , maximal rate of tension redevelopment at pCa 4.5; n_H , Hill coefficient for Ca²⁺-activated tension–pCa relationship; pCa_{50} , pCa required for half-maximal activation; P_{rest} , Ca²⁺-independent tension at pCa 9.0; P_o , maximal Ca²⁺-activated tension at pCa 4.5; P_{Tot} , maximal Ca²⁺-activated tension (maximal Ca²⁺-activated tension plus Ca²⁺-independent tension).

^aSignificantly different from WT and FT-WT mice ($P < 0.05$).

ChemiDoc MP System (Bio-Rad). Densitometric analysis was performed using Image Lab software (Bio-Rad), with the intensity ratio of the IOD of the cMyBP-C band to the IOD of the corresponding β -actin band calculated to correct for loading and to permit comparison between samples. All cMyBP-C/ β -actin intensity ratios were normalized to WT values.

RNA analysis

Total RNA was isolated from frozen WT, FT-WT, and cMyBP-C null ventricles, as described previously (Farrell et al., 2018). The frozen ventricles were homogenized using TRIzol reagent (Ambion) purified with the Mini Total RNA kit (IBI Scientific) and quantified spectrophotometrically. Reverse transcription of total RNA was performed using the iScript Reverse Transcription Supermix for reverse transcription quantitative PCR (Bio-Rad) to generate

complementary DNA. Gene expression was assessed using the TaqMan Gene Expression Master Mix (Applied Biosystems) for myosin binding protein C (*MYBPC3*, Mm00435104_m1), atrial natriuretic peptide (*Nppa*, Mm00435104_m1), brain natriuretic peptide (*Nppb*, Mm00435104_m1), and β -actin (*Actb*, Mm00607939_s1). Real-time monitoring of TaqMan fluorescence was performed on the Stratagene Mx3005P qPCR system (Agilent Technologies). Data were analyzed using Microsoft Excel, with the relative levels of mRNA expression normalized to *Actb* expression according to the $\Delta\Delta C_T$ method.

Statistical analysis

All data are presented as means ± SEM. Statistical analyses were performed using a one-way ANOVA followed by the Holm–Sidak post hoc test for multiple comparisons with significance set at the $P < 0.05$ level. For data collected serially using the same experimental animals, statistical analyses were performed using a two-way ANOVA followed by the Holm–Sidak post hoc test for multiple comparisons versus the noninduced FT-WT at baseline (i.e., $t = 0$). Normality was confirmed using the Shapiro–Wilk test with significance set at the $P < 0.01$ level.

Results

Do noninduced FT-WT mice exhibit a WT phenotype?

Confirmation of cMyBP-C expression in FT-WT mice

Three FT-WT sublines, designated as 2252, 2254, and 2267, were generated as a consequence of the initial breeding program (Fig. 1). At 3 mo of age, FT-WT mice ($tTA^{+/0}$, $tResp^{+/0}$, $cMyBP-C^{-/-}$) from each subline were subjected to echocardiographic analysis to assess in vivo LV functional status and were then examined for transgenic expression of cMyBP-C (Fig. 2). Consistent with our previously published results (Harris et al., 2002; Chen et al., 2012), EF (Fig. 2A) and ET (Fig. 2B) were significantly reduced in cMyBP-C null mice, whereas IVRT (Fig. 2C) was significantly prolonged. Although mice from FT-WT sublines 2252 and 2254

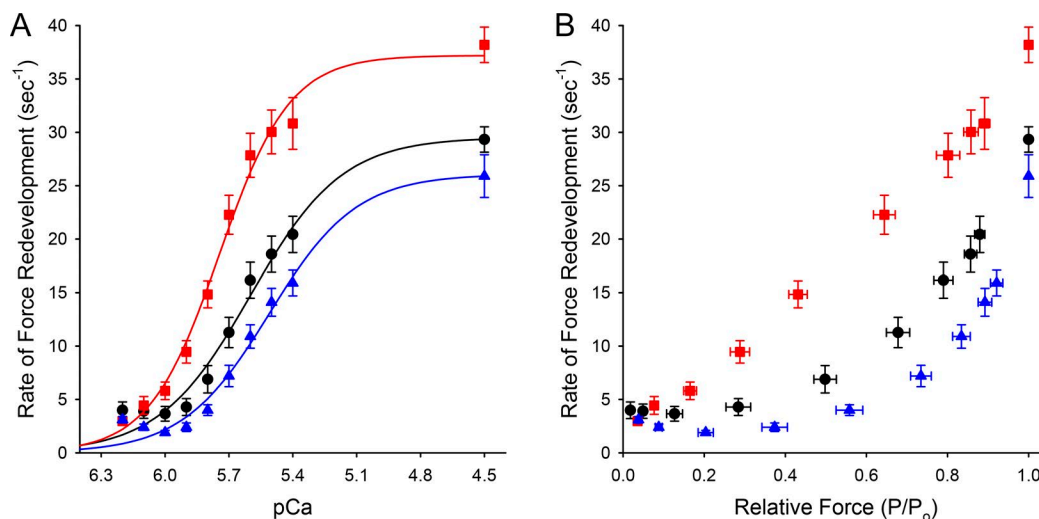


Figure 6. FT-WT skinned trabeculae exhibit normal cross-bridge cycling kinetics. (A and B) The Ca²⁺-dependence (A) and activation-dependence (B) of the rate of force redevelopment following rapid release and restretch were measured in skinned trabeculae from WT (triangle), FT-WT (circle), and cMyBP-C null (square) mice. All values represent mean, and error bars represent ±SEM.

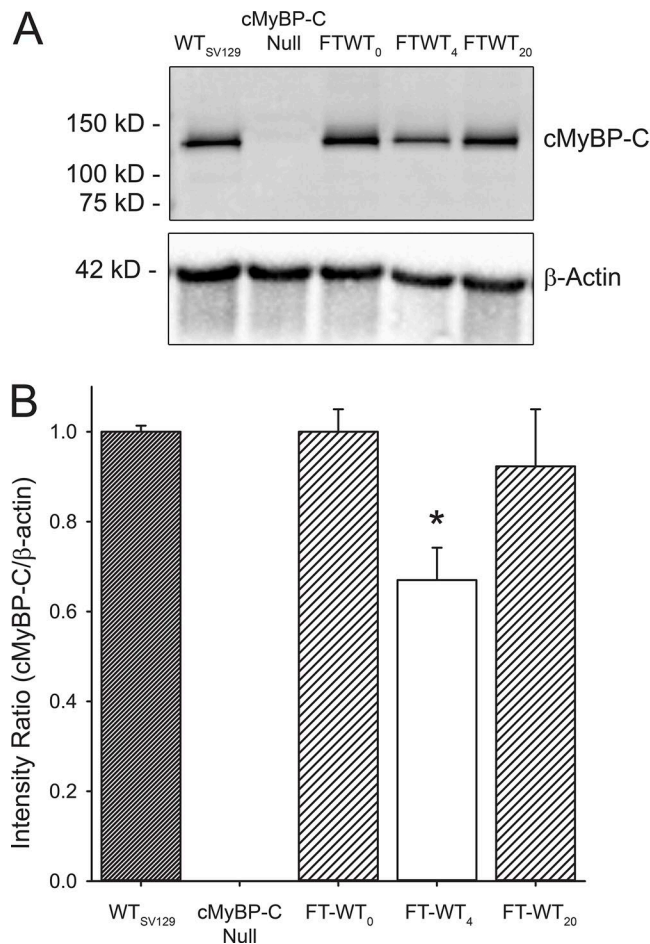


Figure 7. Reversible expression of cMyBP-C in FT-WT myocardium. (A) Representative Western blot of myofibrils isolated from WT, cMyBP-C null, and FT-WT myocardium: noninduced (FT-WT₀), during 4 wk of dietary doxycycline supplementation (FT-WT₄), and following withdrawal of doxycycline (FT-WT₂₀). **(B)** Densitometric analysis of the expression of cMyBP-C relative to β -actin (intensity ratio) and normalized to WT values. All values represent mean, and error bars represent \pm SEM, with $n = 8$ hearts per group. *, $P < 0.05$ significant difference compared with WT mice at baseline.

were genotyped as positive for both the tTA and tResp transgenes, these animals exhibited depressed LV function similar to that observed in the cMyBP-C null mice. In contrast, mice from FT-WT subline 2267 exhibited normal cardiac function, as the indices of EF (Fig. 2 A), ET (Fig. 2 B), and IVRT (Fig. 2 C) were indistinguishable from values observed in WT mice. SDS-PAGE was used subsequently to quantify the level of cMyBP-C transgenic expression in the three FT-WT sublines. As demonstrated in Fig. 2 D, sublines 2252 and 2254 exhibited very low (<10%) levels of cMyBP-C. However, subline 2267 demonstrated near-stoichiometric (~98%) expression of cMyBP-C when compared with WT values and was thus selected for experimental use.

Reverse transcription quantitative PCR was performed to assess cMyBP-C mRNA expression in FT-WT, WT, and cMyBP-C null hearts (Fig. 3). No significant differences were observed in *MYBPC3* mRNA expression between FT-WT and WT myocardium, a result consistent with previous work using a cMyBP-C overexpression model (Yang et al., 1998). However, a trend toward increased mRNA expression of *Nppa* and *Nppb* was noted

in the FT-WT myocardium. In contrast, *Nppa* and *Nppb* were significantly elevated in the cMyBP-C null myocardium, as reported previously (Harris et al., 2002; Chen et al., 2012).

Cardiac histology and sarcomeric incorporation of cMyBP-C

To study the structural and morphological phenotypes elicited by the transgenic expression of cMyBP-C, histological analyses were performed on cardiac sections from FT-WT mice. Neither hematoxylin and eosin staining nor Masson's trichrome revealed any significant abnormalities in the FT-WT sections compared with WT (Fig. 4). As anticipated, cMyBP-C null hearts exhibited a significantly higher percentage of areas of fibrosis ($35.0 \pm 1.4\%$, $P < 0.05$) than that observed in WT ($7.6 \pm 1.0\%$) and FT-WT ($12.7 \pm 5.1\%$) hearts. Furthermore, transgenically expressed cMyBP-C appeared to be appropriately positioned within the FT-WT myocardium. Immunofluorescent labeling of myofibrils with anti-cMyBP-C/Alexa Fluor 488 demonstrated characteristic A-band doublets corresponding to cMyBP-C in both WT and FT-WT myocardium, but not in cMyBP-C null myocardium (Fig. 4).

Steady-state force and cross-bridge cycling kinetics in FT-WT. The skinned myocardium isolated from FT-WT and WT mice exhibited similar steady-state force responses to activating calcium (Fig. 5, A and B). Table 1 summarizes the values of maximal total force (P_{Tot}), maximal Ca^{2+} -activated force (P_o), Ca^{2+} -independent force (P_{rest}), the Ca^{2+} sensitivity of force (pCa_{50}), and the steepness of the force-pCa relationship (n_H) measured in skinned trabeculae isolated from WT, FT-WT, and cMyBP-C null hearts. Both WT and FT-WT skinned myocardium exhibited similar Ca^{2+} - and activation-dependent (Fig. 6 A and B) increases in the rate constant of force redevelopment (k_{tr}). Increasing Ca^{2+} from pCa 6.2 to pCa 4.5 progressively increased k_{tr} from 4.0 ± 0.8 to 29.3 ± 1.2 s⁻¹ in FT-WT myocardium and from 3.1 ± 0.3 to 25.9 ± 2.0 s⁻¹ in WT myocardium. However, at submaximal and maximal levels of activation, k_{tr} was significantly faster in cMyBP-C null myocardium than in either WT or FT-WT myocardium, a result consistent with previous findings in cMyBP-C null and WT myocardium (Korte et al., 2003; Chen et al., 2010; Merkulov et al., 2012).

Are the depressed in vivo functional phenotypes associated with partial knockdown of cMyBP-C reversible in inducible FT-WT mice?

Partial knockdown and reexpression of cMyBP-C

To elicit the transient knockdown of cMyBP-C expression, FT-WT mice of either sex were fed normal rodent chow supplemented with doxycycline for a total of 4 wk. Reexpression of cMyBP-C in FT-WT mice was induced by returning these animals to a diet of normal rodent chow for 16 wk. Fig. 7 A shows a representative Western blot of myofibrillar proteins isolated from (1) noninduced FT-WT hearts (FT-WT₀), (2) following 4 wk of doxycycline treatment (FT-WT₄), and (3) following 4 wk of doxycycline treatment and 16 wk of recovery (FT-WT₂₀). cMyBP-C null and WT myofibrillar samples were included as controls. cMyBP-C expression in the noninduced FT-WT myocardium did not differ significantly from WT myocardium. However, following 4 wk of doxycycline diet supplementation, cMyBP-C levels decreased by ~35% in the FT-WT₄ myocardium (Fig. 7 B). Reintroduction of normal rodent chow resulted in the near-complete recovery of

Table 2. Summary of M-mode echocardiographic measurements

	WT _{SV129} (12)	FT-WT ₀ (8)	FT-WT ₂ (8)	FT-WT ₄ (8)	FT-WT ₅ (8)	FT-WT ₈ (8)	FT-WT ₁₂ (8)	FT-WT ₂₀ (8)	cMyBP-C null (10)
Body weight (g)	29.2 ± 1.1	23.7 ± 1.5	24.5 ± 1.5	24.2 ± 1.2	24.6 ± 1.4	24.8 ± 1.4	25.1 ± 1.3	27.0 ± 1.4	23.2 ± 1.0
Diet	Control	Control	Dox	Dox	Dox	Dox	Dox	Dox	Control
Time course		0 wk	2 wk	4 wk	4 wk	4 wk	4 wk	4 wk	
Diet					Control	Control	Control	Control	
Time course					1 wk	4 wk	8 wk	16 wk	
LV morphology									
LVID _d (mm)	3.77 ± 0.05	3.95 ± 0.14	4.12 ± 0.13	4.38 ± 0.12	4.60 ± 0.13	4.41 ± 0.13	4.45 ± 0.20	4.14 ± 0.08	5.08 ± 0.13 ^a
LVID _s (mm)	2.49 ± 0.08	2.66 ± 0.16	2.83 ± 0.12	3.37 ± 0.13	3.66 ± 0.11	3.38 ± 0.16	3.45 ± 0.20	3.06 ± 0.13	4.25 ± 0.14 ^a
LVPW _d (mm)	0.66 ± 0.06	0.76 ± 0.01	0.82 ± 0.02	0.85 ± 0.01	0.85 ± 0.01	0.90 ± 0.01	0.91 ± 0.03	0.96 ± 0.02	0.83 ± 0.03 ^a
LVPW _s (mm)	1.18 ± 0.04	1.19 ± 0.03	1.24 ± 0.03	1.14 ± 0.03	1.09 ± 0.04	1.23 ± 0.05	1.21 ± 0.03	1.24 ± 0.05	1.14 ± 0.04
LVAW _d (mm)	0.65 ± 0.02	0.76 ± 0.02	0.83 ± 0.02	0.86 ± 0.02	0.88 ± 0.01	0.91 ± 0.02	0.91 ± 0.02	0.96 ± 0.04	0.82 ± 0.03 ^a
LVAW _s (mm)	1.10 ± 0.04	1.22 ± 0.04	1.35 ± 0.05	1.27 ± 0.06	1.26 ± 0.03	1.40 ± 0.04	1.34 ± 0.05	1.34 ± 0.05	1.09 ± 0.05
LV volume _d (μl)	61.3 ± 2.0	64.3 ± 7.2	79.6 ± 5.5	88.7 ± 5.7	97.6 ± 6.4	95.0 ± 9.1	96.8 ± 10.1	76.3 ± 3.7	123.7 ± 7.5 ^a
LV volume _s (μl)	20.8 ± 1.8	24.6 ± 4.3	35.5 ± 5.1	44.6 ± 5.5	51.9 ± 6.0	47.7 ± 5.5	50.7 ± 6.7	37.3 ± 3.7	81.7 ± 6.4 ^a
LV mass (mg)	89.3 ± 2.4	108.9 ± 6.2	135.2 ± 9.1	146.1 ± 5.4	160.0 ± 10.2	174.4 ± 11.4	170.8 ± 10.8	149.0 ± 10.4	180.7 ± 8.9 ^a
LV/BW (mg/g)	3.0 ± 0.1	4.4 ± 0.4	5.6 ± 0.3	6.1 ± 0.2	6.6 ± 0.4	7.1 ± 0.5	6.8 ± 0.3	5.6 ± 0.1	7.6 ± 0.3 ^a
LV function									
EF (%)	64.8 ± 1.8	63.2 ± 3.0	56.5 ± 3.2	47.6 ± 4.4 ^a	42.7 ± 1.4 ^a	49.0 ± 1.5 ^a	48.5 ± 3.3 ^a	52.1 ± 2.5	33.0 ± 3.8 ^a
EnFS (%)	33.6 ± 1.1	34.0 ± 2.1	29.5 ± 2.1	24.1 ± 2.5 ^a	21.0 ± 0.8 ^a	25.4 ± 0.9 ^a	24.6 ± 2.0 ^a	26.6 ± 1.5	16.0 ± 2.0 ^a
IVRT (ms)	20.9 ± 1.0	20.4 ± 1.1	23.5 ± 0.7	27.0 ± 0.6 ^a	27.5 ± 1.3 ^a	28.4 ± 2.0 ^a	26.0 ± 1.9 ^a	22.2 ± 1.3	30.5 ± 1.1 ^a
ET (ms)	43.7 ± 1.2	41.9 ± 1.4	40.6 ± 1.3	37.9 ± 0.6	34.1 ± 0.9 ^a	33.6 ± 1.4 ^a	35.9 ± 1.3 ^a	40.4 ± 1.4	33.5 ± 0.9 ^a
Heart rate (bpm)	466 ± 16	451 ± 16	446 ± 13	458 ± 22	459 ± 15	469 ± 12	475 ± 20	470 ± 20	461 ± 13

All values are expressed as means ± SEM, with the number of mice listed in parentheses. LV mass was calculated as $1.053 \times [(LVID_d + LVPW_d + LVAW_d)^3 - (LVID_s)^3]$. Dox, doxycycline; EnFS, endocardial fractional shortening; LVID, left ventricular internal dimension; LVAW, left ventricular anterior wall.

^aSignificantly different compared to noninduced FT-WT and WT mice ($P < 0.05$).

cMyBP-C expression in the FT-WT₂₀ myocardium to levels measured in the noninduced FT-WT myocardium (Fig. 7B).

LV function in response to the partial knockdown and reexpression of cMyBP-C

To assess ventricular function following the knockdown and subsequent reexpression of cMyBP-C, serial echocardiograms were collected from FT-WT mice. Summary data from echocardiographic measurements are listed in Table 2. LV function in noninduced FT-WT mice was not statistically different from that in WT mice, whereas LV function was significantly depressed in cMyBP-C null mice. Following 4 wk of doxycycline-diet supplementation and the concomitant reduction in cMyBP-C expression (Fig. 7B), both EF (Fig. 8A) and ET (Fig. 8B) were decreased, and IVRT was increased (Fig. 8C). Furthermore, both the LV internal dimension during diastole (Fig. 8D) and LV posterior wall thickness were increased (Table 2). It should be noted that LV function continued to decrease during the first week of return to a normal diet before gradually increasing over the ensuing 3–8 wk. Orally administered doxycycline has a reported half-life of 14–24 h (Perdue and Standiford, 1999). Thus, it is reasonable to presume that a minimum of 2 wk would be required to reduce

plasma doxycycline to negligible levels, at which point the inhibition of the tTA transgene would cease and robust transgenic expression of cMyBP-C would resume. Ultimately, the partial knockdown of cMyBP-C expression was completely reversed and was accompanied by the near recovery of normal LV function.

Discussion

The loss of cMyBP-C has been linked to LV dilation, cardiac hypertrophy, and impaired ventricular function in both cMyBP-C constitutive and conditional knockout mice. The present study was designed to determine whether the structural and functional phenotypes evident in the MYBPC3 null mouse are reversible. To test this idea, we generated a cardiac-specific inducible transgenic mouse model to examine the in vivo LV functional effects associated with the reversible expression of WT cMyBP-C. The use of constitutive and conditional cMyBP-C knockout mouse models in previous studies (Harris et al., 2002; Chen et al., 2012) demonstrated a significant impairment of cardiac function related to the loss of cMyBP-C. Both types of knockout mouse models are excellent platforms to study disease-related processes associated with the loss of cMyBP-C. In contrast, the use of the

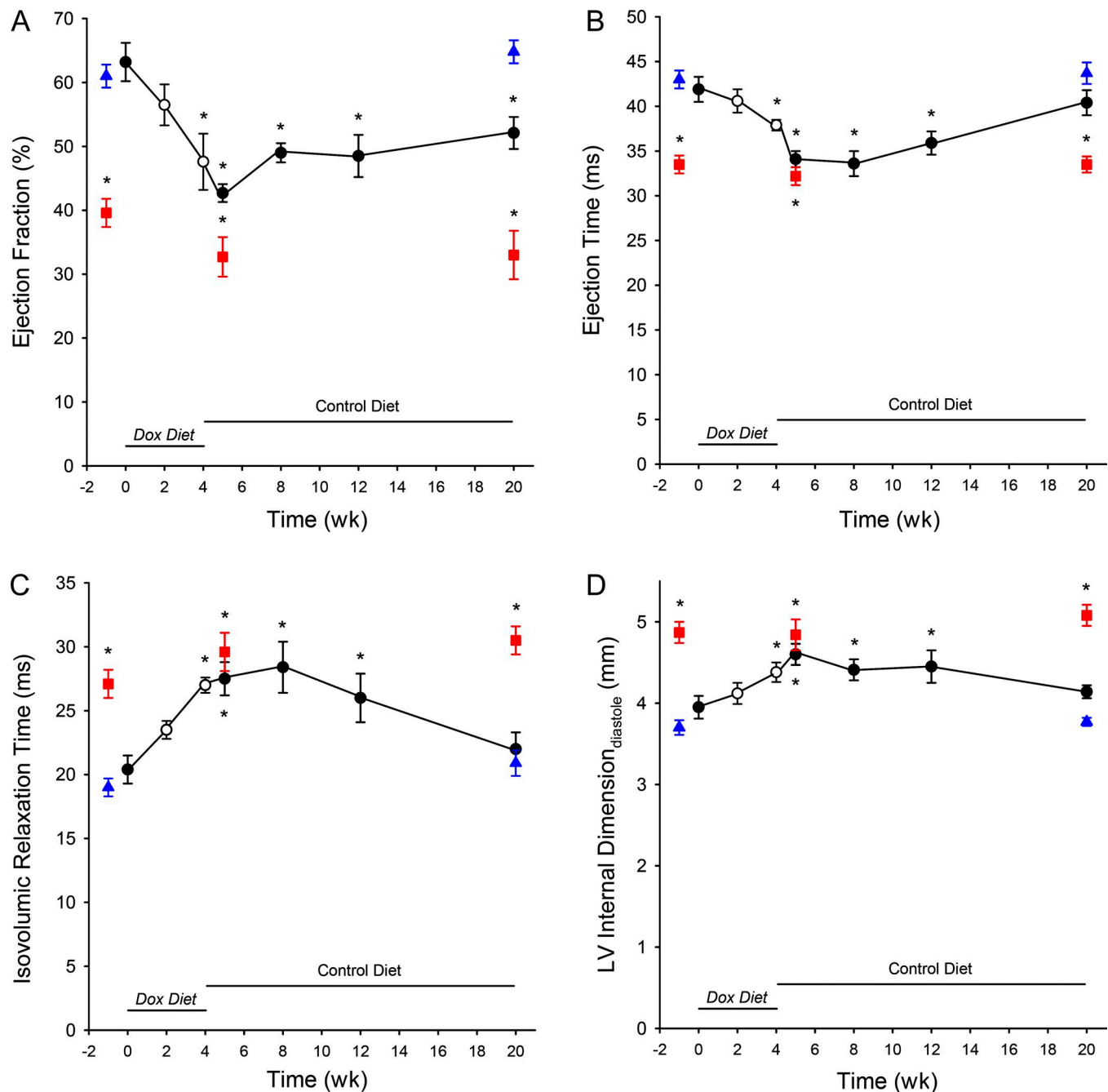


Figure 8. **Analysis of in vivo LV function of FT-WT mice during partial knockdown and subsequent reexpression of cMyBP-C.** (A–D) Time-course echocardiographic analysis of EF (A), ET (B), IVRT (C), and LV internal dimension (D) during diastole in WT (triangle, $n = 12$), cMyBP-C null (square, $n = 10$), and FT-WT (closed circle, control diet; open circle, doxycycline [Dox] diet, $n = 8$) mice. All values represent means, and error bars represent \pm SEM. *, $P < 0.05$ significant difference compared with noninduced FT-WT mice at baseline ($t = 0$), $P < 0.05$.

Tet-Off inducible system not only allows for controlled, reversible expression of cMyBP-C but also provides experimental flexibility in terms of determining the age (e.g., neonate vs. adult) at which knockdown occurs and the length of time of the knockdown before reexpression of cMyBP-C.

The main objectives of this proof-of-concept study were straightforward. First, do the noninduced FT-WT mice exhibit a WT phenotype? Second, is the reversible knockdown and subsequent reexpression of cMyBP-C accompanied by concomitant

changes in LV function? Both questions must be answered affirmatively in order to establish the feasibility of using the inducible FT-WT mouse model to investigate disease-related processes associated with the down-regulation of cMyBP-C expression. With regard to the first question, the FT-WT did display a WT phenotype. Relative to WT controls, the FT-WT mice exhibited (1) near-identical levels of cMyBP-C expression, (2) a normal cardiac histological profile, (3) appropriate sarcomeric incorporation of cMyBP-C, (4) similar steady-state force development and activation-dependent

(i.e., Ca^{2+} and force) increases in the rate of force redevelopment, and (5) comparable in vivo LV functional indices. Having established the WT functional phenotype of FT-WT mice, we then investigated whether the depressed functional phenotypes associated with the cMyBP-C null mice are reversible following reexpression of cMyBP-C. After 4 wk of doxycycline treatment, the expression of cMyBP-C was reduced by ~35% and was accompanied by significant LV dysfunction, an effect consistent with that observed in other mouse models of cMyBP-C knockdown (Chen et al., 2012; Cheng et al., 2013). Upon withdrawal of doxycycline, LV functional indices continued to decrease during the first week of recovery and gradually improved over the ensuing 8 wk. This observation was anticipated, since it was estimated that a minimum of 2 wk would be needed for effective clearance of doxycycline (Perdue and Standiford, 1999). Thus, the overall reexpression of cMyBP-C reflects a balance between the transactivator turning on the responder transgene versus the transactivator itself being inhibited by the presence of doxycycline. It was expected that during the first few weeks of recovery, the inhibitory effect of doxycycline would continually diminish and then vanish, leading to a progressive increase in the transgenic expression of cMyBP-C, subsequent reincorporation of cMyBP-C into the sarcomere, and the recovery of LV function to levels near that observed in noninduced FT-WT mice. The results in the current study demonstrating that diminished LV functional capacity can be rescued with the reexpression of cMyBP-C provide definitive evidence for similar conclusions by Merkulov et al. (2012), who used in vivo gene transfer to increase cMyBP-C expression and improve contractile function in cMyBP-C null mice.

In contrast to that observed in the conditional knockdown of cMyBP-C (Chen et al., 2012), doxycycline treatment resulted in LV internal dimension (LVID_d) and hypertrophy of the LV wall (LVPW_d; Table 2), mimicking generally the HCM phenotype previously reported in cMyBP-C null mice (Harris et al., 2002; Carrier et al., 2004). In the current study, it is unclear if the knockdown of cMyBP-C is the sole mediating factor eliciting LV dilation and cardiac hypertrophy or whether additional factors contribute to this response. It has been reported that chronic exposure to doxycycline can attenuate matrix metalloproteinase expression and activity, resulting in adverse LV remodeling in models of LV hypertrophy (Curci et al., 2000; Spinale et al., 2006). These effects can be observed even after 4 wk of doxycycline treatment (Vinet et al., 2008). In the current study, LV posterior wall thickness remained elevated throughout the recovery phase, whereas LV internal dimensions returned to values approximating those observed in the noninduced FT-WT mice (Fig. 8 D; Table 2).

In summary, cMyBP-C expression in the FT-WT myocardium did not differ significantly from that measured in WT myocardium. The stoichiometric expression of cMyBP-C in the FT-WT mice produced a WT-like phenotype in terms of normal LV function and cardiac structure. The doxycycline-induced loss of cMyBP-C in FT-WT mice elicited significant ventricular functional (EF, ET, and IVRT) and structural (LVPW and LVID) derangements that were effectively reversed after the withdrawal of doxycycline and subsequent reexpression of cMyBP-C. Therefore, the data collected in this proof-of-concept study support the use of the doxycycline-inducible, controlled transgenic expression system

to study the role of WT cMyBP-C in regulating normal systolic and diastolic ventricular function across the life span (i.e., neonate, adult, and senescent). Furthermore, the doxycycline-inducible system could be used to study the functional consequences associated with HCM-related mutations in cMyBP-C. For example, the doxycycline-mediated inhibition of the WT transgene on an MYBPC3 HCM mutant background would allow for the expression of mutant cMyBP-C, resulting in LV dysfunction and cardiac remodeling. Subsequent withdrawal of doxycycline would induce the reexpression of the WT cMyBP-C transgene, thereby potentially rescuing the HCM-related phenotype.

Acknowledgments

We thank Dr. Jeff Robbins (Cincinnati Children's Hospital) for his gift of the tTA mice, Dr. Timothy Hacker (University of Wisconsin Cardiovascular Research Center) for echocardiography services, and Jennifer Wachholz, Elizabeth Vang, and Megan Doty for technical assistance.

This work was supported by the National Heart, Lung, and Blood Institute (grants R37-HL082900 and RO1-HL139883 to R.L. Moss).

The authors declare no competing financial interests.

Author contributions: D.P. Fitzsimons and R.L. Moss designed the study; J.A. Giles, J.R. Patel, A. Miller, and E. Iverson collected the data; J.A. Giles, J.R. Patel, and D.P. Fitzsimons analyzed the data; D.P. Fitzsimons and R.L. Moss wrote the manuscript; all authors reviewed the manuscript.

Henk L. Granzier served as editor.

Submitted: 31 August 2018

Accepted: 27 November 2018

References

- Ababou, A., M. Gautel, and M. Pfuhl. 2007. Dissecting the N-terminal myosin binding site of human cardiac myosin-binding protein C. Structure and myosin binding of domain C2. *J. Biol. Chem.* 282:9204–9215. <https://doi.org/10.1074/jbc.M610899200>
- Ababou, A., E. Rostkova, S. Mistry, C. Le Masurier, M. Gautel, and M. Pfuhl. 2008. Myosin binding protein C positioned to play a key role in regulation of muscle contraction: structure and interactions of domain C1. *J. Mol. Biol.* 384:615–630. <https://doi.org/10.1016/j.jmb.2008.09.065>
- Bennett, P.M., D.O. Fürst, and M. Gautel. 1999. The C-protein (myosin binding protein C) family: regulators of contraction and sarcomere formation? *Rev. Physiol. Biochem. Pharmacol.* 138:203–234. <https://doi.org/10.1007/BF0119628>
- Bezold, K.L., J.F. Shaffer, J.K. Khosha, E.R. Hoye, and S.P. Harris. 2013. A gain-of-function mutation in the M-domain of cardiac myosin-binding protein-C increases binding to actin. *J. Biol. Chem.* 288:21496–21505. <https://doi.org/10.1074/jbc.M113.474346>
- Bhuiyan, M.S., P. McLendon, J. James, H. Osinska, J. Gulick, B. Bhandary, J.N. Lorenz, and J. Robbins. 2016. In vivo definition of cardiac myosin-binding protein C's critical interactions with myosin. *Pflugers Arch.* 468:1685–1695. <https://doi.org/10.1007/s00424-016-1873-y>
- Carrier, L., R. Knöll, N. Vignier, D.I. Keller, P. Bausero, B. Prudhon, R. Isnard, M.L. Ambroisine, M. Fiszman, J. Ross Jr., et al. 2004. Asymmetric septal hypertrophy in heterozygous cMyBP-C null mice. *Cardiovasc. Res.* 63:293–304. <https://doi.org/10.1016/j.cardiores.2004.04.009>
- Carrier, L., G. Mearini, K. Stathopoulou, and F. Cuello. 2015. Cardiac myosin-binding protein C (MYBPC3) in cardiac pathophysiology. *Gene.* 573:188–197. <https://doi.org/10.1016/j.gene.2015.09.008>

- Chen, P.P., J.R. Patel, I.N. Rybakova, J.W. Walker, and R.L. Moss. 2010. Protein kinase A-induced myofilament desensitization to Ca^{2+} as a result of phosphorylation of cardiac myosin-binding protein C. *J. Gen. Physiol.* 136:615–627. <https://doi.org/10.1085/jgp.201010448>
- Chen, P.P., J.R. Patel, P.A. Powers, D.P. Fitzsimons, and R.L. Moss. 2012. Dissociation of structural and functional phenotypes in cardiac myosin-binding protein C conditional knockout mice. *Circulation*. 126:1194–1205. <https://doi.org/10.1161/CIRCULATIONAHA.111.089219>
- Cheng, Y., X. Wan, T.A. McElfresh, X. Chen, K.S. Gresham, D.S. Rosenbaum, M.P. Chandler, and J.E. Stelzer. 2013. Impaired contractile function due to decreased cardiac myosin binding protein C content in the sarcomere. *Am. J. Physiol. Heart Circ. Physiol.* 305:H52–H65. <https://doi.org/10.1152/ajpheart.00929.2012>
- Curci, J.A., D. Mao, D.G. Bohner, B.T. Allen, B.G. Rubin, J.M. Reilly, G.A. Sicard, and R.W. Thompson. 2000. Preoperative treatment with doxycycline reduces aortic wall expression and activation of matrix metalloproteinases in patients with abdominal aortic aneurysms. *J. Vasc. Surg.* 31:325–342. [https://doi.org/10.1016/S0741-5214\(00\)90163-0](https://doi.org/10.1016/S0741-5214(00)90163-0)
- de Lange, W.J., A.C. Grimes, L.F. Hegge, and J.C. Ralphe. 2013. Ablation of cardiac myosin-binding protein-C accelerates contractile kinetics in engineered cardiac tissue. *J. Gen. Physiol.* 141:73–84. <https://doi.org/10.1085/jgp.201210837>
- Fabiato, A. 1988. Computer programs for calculating total from specified free or free from specified total ionic concentrations in aqueous solutions containing multiple metals and ligands. *Methods Enzymol.* 157:378–417. [https://doi.org/10.1016/0076-6879\(88\)57093-3](https://doi.org/10.1016/0076-6879(88)57093-3)
- Farrell, E., A.E. Armstrong, A.C. Grimes, F.J. Naya, W.J. de Lange, and J.C. Ralphe. 2018. Transcriptome analysis of cardiac hypertrophic growth in MYBPC3-null mice suggests early responders in hypertrophic remodeling. *Front. Physiol.* 9:1442. <https://doi.org/10.3389/fphys.2018.01442>
- Fitzsimons, D.P., J.R. Patel, K.S. Campbell, and R.L. Moss. 2001. Cooperative mechanisms in the activation dependence of the rate of force development in rabbit skinned skeletal muscle fibers. *J. Gen. Physiol.* 117:133–148. <https://doi.org/10.1085/jgp.117.2.133>
- Flashman, E., C. Redwood, J. Moolman-Smook, and H. Watkins. 2004. Cardiac myosin binding protein C: its role in physiology and disease. *Circ. Res.* 94:1279–1289. <https://doi.org/10.1161/01.RES.0000127175.21818.C2>
- Godt, R.E., and B.D. Lindsey. 1982. Influence of temperature upon contractile activation and isometric force production in mechanically skinned muscle fibers of the frog. *J. Gen. Physiol.* 80:279–297. <https://doi.org/10.1085/jgp.80.2.279>
- Gresham, K.S., R. Mamidi, J. Li, H. Kwak, and J.E. Stelzer. 2017. Sarcomeric protein modification during adrenergic stress enhances cross-bridge kinetics and cardiac output. *J. Appl. Physiol.* 122:520–530. <https://doi.org/10.1152/japplphysiol.00306.2016>
- Gruen, M., and M. Gautel. 1999. Mutations in beta-myosin S2 that cause familial hypertrophic cardiomyopathy (FHC) abolish the interaction with the regulatory domain of myosin-binding protein-C. *J. Mol. Biol.* 286:933–949. <https://doi.org/10.1006/jmbi.1998.2522>
- Gulick, J., and J. Robbins. 2005. Regulation of transgene expression using tetracycline. *Curr. Protoc. Mol. Biol.* 23:12.1–12.8.
- Harris, S.P., C.R. Bartley, T.A. Hacker, K.S. McDonald, P.S. Douglas, M.L. Greaser, P.A. Powers, and R.L. Moss. 2002. Hypertrophic cardiomyopathy in cardiac myosin binding protein-C knockout mice. *Circ. Res.* 90:594–601. <https://doi.org/10.1161/01.RES.0000012222.70819.64>
- Harris, S.P., R.G. Lyons, and K.L. Bezold. 2011. In the thick of it: HCM-causing mutations in myosin binding proteins of the thick filament. *Circ. Res.* 108:751–764. <https://doi.org/10.1161/CIRCRESAHA.110.231670>
- Kampourakis, T., Z. Yan, M. Gautel, Y.B. Sun, and M. Irving. 2014. Myosin binding protein-C activates thin filaments and inhibits thick filaments in heart muscle cells. *Proc. Natl. Acad. Sci. USA*. 111:18763–18768. <https://doi.org/10.1073/pnas.1413922112>
- Kensler, R.W., R. Craig, and R.L. Moss. 2017. Phosphorylation of cardiac myosin binding protein C releases myosin heads from the surface of cardiac thick filaments. *Proc. Natl. Acad. Sci. USA*. 114:E1355–E1364. <https://doi.org/10.1073/pnas.1614020114>
- Korte, F.S., K.S. McDonald, S.P. Harris, and R.L. Moss. 2003. Loaded shortening, power output, and rate of force redevelopment are increased with knockout of cardiac myosin binding protein-C. *Circ. Res.* 93:752–758. <https://doi.org/10.1161/01.RES.0000096363.85588.9A>
- Mamidi, R., K.S. Gresham, J. Li, and J.E. Stelzer. 2017. Cardiac myosin binding protein-C Ser³⁰² phosphorylation regulates cardiac β -adrenergic reserve. *Sci. Adv.* 3:e1602445. <https://doi.org/10.1126/sciadv.1602445>
- McConnell, B.K., K.A. Jones, D. Fatkin, L.H. Arroyo, R.T. Lee, O. Aristizabal, D.H. Turnbull, D. Georgakopoulos, D. Kass, M. Bond, et al. 1999. Dilated cardiomyopathy in homozygous myosin-binding protein-C mutant mice. *J. Clin. Invest.* 104:1235–1244. <https://doi.org/10.1172/JCI7377>
- Merkulov, S., X. Chen, M.P. Chandler, and J.E. Stelzer. 2012. In vivo cardiac myosin binding protein C gene transfer rescues myofilament contractile dysfunction in cardiac myosin binding protein C null mice. *Circ Heart Fail.* 5:635–644. <https://doi.org/10.1161/CIRCHEARTFAILURE.112.968941>
- Mun, J.Y., M.J. Previs, H.Y. Yu, J. Gulick, L.S. Tobacman, S. Beck Previs, J. Robbins, D.M. Warshaw, and R. Craig. 2014. Myosin-binding protein C displaces tropomyosin to activate cardiac thin filaments and governs their speed by an independent mechanism. *Proc. Natl. Acad. Sci. USA*. 111:2170–2175. <https://doi.org/10.1073/pnas.1316001111>
- Offer, G., C. Moos, and R. Starr. 1973. A new protein of the thick filaments of vertebrate skeletal myofibrils. Extractions, purification and characterization. *J. Mol. Biol.* 74:653–676. [https://doi.org/10.1016/0022-2836\(73\)90055-7](https://doi.org/10.1016/0022-2836(73)90055-7)
- Patel, J.R., J.M. Pleitner, R.L. Moss, and M.L. Greaser. 2012. Magnitude of length-dependent changes in contractile properties varies with titin isoform in rat ventricles. *Am. J. Physiol. Heart Circ. Physiol.* 302:H697–H708. <https://doi.org/10.1152/ajpheart.00800.2011>
- Patel, J.R., G.P. Barton, R.K. Braun, K.N. Goss, K. Haraldsdottir, A. Hopp, G. Diffie, T.A. Hacker, R.L. Moss, and M.W. Eldridge. 2017. Altered right ventricular mechanical properties are afterload dependent in a rodent model of bronchopulmonary dysplasia. *Front. Physiol.* 8:840. <https://doi.org/10.3389/fphys.2017.00840>
- Perdue, B.E., and H.C. Standiford. 1999. Tetracyclines. In *Antimicrobial therapy and vaccines*. V.L. Lu, T.C. Merigan, and S.L. Barriere, editors. Williams & Wilkins, Baltimore, Md. 981–995.
- Previs, M.J., S. Beck Previs, J. Gulick, J. Robbins, and D.M. Warshaw. 2012. Molecular mechanics of cardiac myosin-binding protein C in native thick filaments. *Science*. 337:1215–1218. <https://doi.org/10.1126/science.1223602>
- Previs, M.J., J.Y. Mun, A.J. Michalek, S.B. Previs, J. Gulick, J. Robbins, D.M. Warshaw, and R. Craig. 2016. Phosphorylation and calcium antagonistically tune myosin-binding protein C's structure and function. *Proc. Natl. Acad. Sci. USA*. 113:3239–3244. <https://doi.org/10.1073/pnas.1522236113>
- Ratti, J., E. Rostkova, M. Gautel, and M. Pfuhl. 2011. Structure and interactions of myosin-binding protein C domain CO: cardiac-specific regulation of myosin at its neck? *J. Biol. Chem.* 286:12650–12658. <https://doi.org/10.1074/jbc.M110.156646>
- Razzaque, M.A., M. Gupta, H. Osinska, J. Gulick, B.C. Blaxall, and J. Robbins. 2013. An endogenously produced fragment of cardiac myosin-binding protein C is pathogenic and can lead to heart failure. *Circ. Res.* 113:553–561. <https://doi.org/10.1161/CIRCRESAHA.113.301225>
- Sadayappan, S., J. Gulick, H. Osinska, D. Barefield, F. Cuello, M. Avkiran, V.M. Lasko, J.N. Lorenz, M. Maillet, J.L. Martin, et al. 2011. A critical function for Ser-282 in cardiac Myosin binding protein-C phosphorylation and cardiac function. *Circ. Res.* 109:141–150. <https://doi.org/10.1161/CIRCRESAHA.111.242560>
- Sanbe, A., J. Gulick, M.C. Hanks, Q. Liang, H. Osinska, and J. Robbins. 2003. Re-engineering inducible cardiac-specific transgenesis with an attenuated myosin heavy chain promoter. *Circ. Res.* 92:609–616. <https://doi.org/10.1161/01.RES.0000065442.64694.9F>
- Spinale, F.G., G.P. Escobar, J.W. Hendrick, L.L. Clark, S.S. Camens, J.P. Minogio, C.G. Squires, R.E. Stroud, and J.S. Ikonomidis. 2006. Chronic matrix metalloproteinase inhibition following myocardial infarction in mice: differential effects on short and long-term survival. *J. Pharmacol. Exp. Ther.* 318:966–973. <https://doi.org/10.1124/jpet.106.104455>
- Tong, C.W., X. Wu, Y. Liu, P.C. Rosas, S. Sadayappan, A. Hudmon, M. Muthuchamy, P.A. Powers, H.H. Valdivia, and R.L. Moss. 2015. Phosphoregulation of cardiac inotropy via myosin binding protein-C during increased pacing frequency or beta1-adrenergic stimulation. *Circ Heart Fail.* 8:595–604. <https://doi.org/10.1161/CIRCHEARTFAILURE.114.001585>
- van Dijk, S.J., K.L. Bezold, and S.P. Harris. 2014. Earning stripes: myosin binding protein-C interactions with actin. *Pflugers Arch.* 466:445–450. <https://doi.org/10.1007/s00424-013-1432-8>
- Van Driest, S.L., V.C. Vasile, S.R. Ommen, M.L. Will, A.J. Tajik, B.J. Gersh, and M.J. Ackerman. 2004. Myosin binding protein C mutations and compound heterozygosity in hypertrophic cardiomyopathy. *J. Am. Coll. Cardiol.* 44:1903–1910. <https://doi.org/10.1016/j.jacc.2004.07.045>
- Vinet, L., P. Rouet-Benzineb, X. Marniquet, N. Pellegrin, L. Mangin, L. Louedec, J.L. Samuel, and J.J. Mercadier. 2008. Chronic doxycycline exposure

- accelerates left ventricular hypertrophy and progression to heart failure in mice after thoracic aorta constriction. *Am. J. Physiol. Heart Circ. Physiol.* 295:H352–H360. <https://doi.org/10.1152/ajpheart.01101.2007>
- Weith, A.E., M.J. Previs, G.J. Hoepflich, S.B. Previs, J. Gulick, J. Robbins, and D.M. Warshaw. 2012a. The extent of cardiac myosin binding protein-C phosphorylation modulates actomyosin function in a graded manner. *J. Muscle Res. Cell Motil.* 33:449–459. <https://doi.org/10.1007/s10974-012-9312-y>
- Weith, A., S. Sadayappan, J. Gulick, M.J. Previs, P. Vanburen, J. Robbins, and D.M. Warshaw. 2012b. Unique single molecule binding of cardiac myosin binding protein-C to actin and phosphorylation-dependent inhibition of actomyosin motility requires 17 amino acids of the motif domain. *J. Mol. Cell. Cardiol.* 52:219–227. <https://doi.org/10.1016/j.yjmcc.2011.09.019>
- Winegrad, S. 1999. Cardiac myosin binding protein C. *Circ. Res.* 84:1117–1126. <https://doi.org/10.1161/01.RES.84.10.1117>
- Yang, Q., A. Sanbe, H. Osinska, T.E. Hewett, R. Klevitsky, and J. Robbins. 1998. A mouse model of myosin binding protein C human familial hypertrophic cardiomyopathy. *J. Clin. Invest.* 102:1292–1300. <https://doi.org/10.1172/JCI3880>